Anode Materials

Deutsche Ausgabe: DOI: 10.1002/ange.201503150
Internationale Ausgabe: DOI: 10.1002/anie.201503150

Energy Storage Materials from Nature through Nanotechnology: A Sustainable Route from Reed Plants to a Silicon Anode for Lithium-Ion Batteries**

*Jun Liu, Peter Kopold, Peter A. van Aken, Joachim Maier, and Yan Yu**

Dedicated to Professor Juri Grin on the occasion of his 60th birthday

Abstract: *Silicon is an attractive anode material in energy storage devices, as it has a ten times higher theoretical capacity than its state-of-art carbonaceous counterpart. However, the common process to synthesize silicon nanostructured electrodes is complex, costly, and energy-intensive. Three-dimensional (3D) porous silicon-based anode materials have been fabricated from natural reed leaves by calcination and magnesiothermic reduction. This sustainable and highly abundant silica source allows for facile production of 3D porous silicon with very good electrochemical performance. The obtained silicon anode retains the 3D hierarchical architecture of the reed leaf. Impurity leaching and gas release during the fabrication process leads to an interconnected porosity and the reductive treatment to an inside carbon coating. Such anodes show a remarkable Li-ion storage performance: even after 4000 cycles and at a rate of 10 C, a specific capacity of 420 mA h g^{-1} is achieved.*

The demand for lithium-ion batteries with high energy, high power density, and high rate capability has substantially increased in view of their use in hybrid electric vehicles, back-up electricity storage units, and lightweight and portable electric devices.[1–3] Carbon-based materials are still the most common anode materials in commercial Li-ion batteries, yet their specific capacity is relatively low (372 mA h g^{-1}) and the rate capability rather poor owing to its insufficient Li^+ diffusion coefficient.[4] Silicon is considered as a most promising candidate for next generation anodes owing to its very high theoretical capacity of 4200 mA h g^{-1} (based on Si and corresponding to $Li_{22}Si_4$) and low operating voltage (about 0.1 V vs. Li/Li^+).[5,6] However, the use of silicon faces major difficulties owing to insufficient transport properties and particularly its large volume expansion (more than 300%) during lithiation.[7] Two main strategies have been developed to improve the structural stability and electrochemical performance of Si anodes. The first strategy is based on structuring the silicon material itself. Si nanostructures, such as Si nanowires, nanotubes, hollow nanospheres, and porous structures, have been designed and successfully synthesized.[8–13] Particularly, Si hollow nanospheres, nanotubes, and 3D porous structures with a large void space can easily accommodate the volume change and relieve the diffusion-induced stress during charge–discharge cycles.[8,9] The other complementary strategy is to apply electronically conductive coatings.[14–21] Such coatings not only improve the transport properties, but may also act as soft media to buffer the stress caused by volume expansion.[17] Carbon coating by thermal decomposition of carbon precursors, silver coating by a silver-mirror reaction, and conductive polymer coatings are well-established methods in this context.[14–18]

While a manifold of silicon-based nanostructured anodes with very good electrochemical performances have been successfully fabricated, most of them lack potential of practical application owing to the high cost of precursors and methodology or the inability to produce materials at gram or even kilogram level.[9–11] Nanostructures derived from the pyrolysis of silane, such as silicon nanospheres, nanotubes, and nanowires, have all demonstrated excellent storage behavior.[9–11] However, synthesis techniques such as chemical vapor deposition of expensive and highly pyrophoric silane require delicate equipment.[22] Metal-assisted chemical etching and electrochemical anodization of crystalline silicon wafers have been investigated extensively as means of producing highly tunable silicon nanowires by templated and non-templated approaches.[23] However, electronic-grade wafers are relatively costly to produce and the quantity of

[*] Prof. Y. Yu
Key Laboratory of Materials for Energy Conversion
Chinese Academy of Sciences, Department of Materials Science and Engineering, University of Science and Technology of China
Hefei, 230026 (China)
E-mail: yanyumse@ustc.edu.cn
Dr. J. Liu, P. Kopold, Prof. P. A. van Aken, Prof. J. Maier, Prof. Y. Yu
Max Planck Institute for Solid State Research
Heisenbergstrasse 1, 70569 Stuttgart (Germany)
Dr. J. Liu
School of Materials Science and Engineering
South China University of Technology, Key Laboratory of Advanced Energy Storage Materials of Guangdong Province
Guangzhou 510641 (China)

[**] This work was financially supported by the Sofja Kovalevskaja award of the Alexander von Humboldt Foundation, by the National Natural Science Foundation of China (No. 21171015, No. 21373195, No. 11202177), the "Recruitment Program of Global Experts", the program for New Century Excellent Talents in University (NCET-12-0515), the Fundamental Research Funds for the Central Universities (WK2060140014, WK2060140016), the Collaborative Innovation Center of Suzhou Nano Science and Technology, and the Max Planck Society. The research leading to these results has received funding from the European Union Seventh Framework Programme [FP7/2007-2013] under grant agreement No. 312483 (ESTEEM2).

Supporting information for this article is available on the WWW under http://dx.doi.org/10.1002/anie.201503150.

nanowires produced by these routes is on the milligram level.[24,25]

The magnesiothermic reduction of SiO_2 is an attractive method to obtain nanostructured Si.[8,15,16] It requires a lower processing temperature and a shorter reaction time, compared to other reduction processes. The magnesiothermic reduction has already been used to produce 3D macroporous or mesoporous Si.[15] Though successfully applied to Si precursors, the preparation process of Si precursors turned out to be complex and time-consuming.[8,15,16] Just recently, Qian and co-workers decreased the magnesiothermic temperature to 200 °C using a molten salt of $AlCl_3$ in an autoclave, while halosilane $SiCl_4$ is still needed as silicon resource.[26] Silica derivation from nature resources is much more sustainable and lower cost.[27–32] Plants can absorb silicon in the form of silicic acid ($Si(OH)_4$ or $Si(OH)_3O^-$) from the soil.[33] The ability of a plant to accumulate silicon varies greatly from species to species (0.1–10 % of shoot dry weight). Silicon accumulation exceeding 4 % is especially common in monocotyledonous plants, and hence in the plant families of Poaceae, Equisetaceae, and Cyperaceae.[34,35] Reeds, as the typical members of the Poaceae family, grow in along rivers, or in shallow water near ponds. They are widely distributed worldwide in the wetland of the temperate regions.[35] As a living plant, reeds absorb silica from soil, and the silica accumulates around cellulose microcompartments.[35,36] Therefore, reeds are suitable natural reservoirs of nanostructured silica and its derivatives. Yet they are not only appropriate Si sources, they also contain silica in a very favorable nanoscale arrangement. Recently, there are some reports about using beach sand[31,32] and rice husks[27–28] as Si sources for producing Si anodes for Li-ion batteries. However, owing to the bulk structure of sea sand and rice husks, only Si nanoparticles were finally arrived at.[27–31] In contrast, reed leaves exhibit well-defined sheet-like 3D hierarchical microstructures, which as we demonstrate can be transformed into a well-suited 3D highly porous hierarchical Si architectures. After having applied a thin carbon layer coating to these 3D Si hierarchical architectures, the finally achieved Si⊂C anode shows high specific capacity, very good rate capability, and cycling stability for advanced Li-ion batteries.

Our synthesis route is based on magnesiothermic reduction of 3D porous SiO_2 converted from natural reed leaves. It utilizes the reed leaf as skeleton template, and the in situ generated MgO by-products as pore template. As shown in Scheme 1 a, which demonstrates various synthesis procedures, the existing methods for producing nanostructured Si anodes are limited to high-temperature/high-energy pyrolysis of silane/halosilane precursors, laser ablation of bulk Si, and metal-assisted etching/electrochemical anodization of high-cost crystalline silicon wafers.[22–24,37–40] In contrast to the established synthesis routes, our route avoids the use of expensive processing needed to produce Si anodes with comparable cost and scalability to graphite anodes. As shown in the flow chart and optical images in Scheme 1 b, natural reed leaves are first converted to 3D porous SiO_2 by thermally decomposing the organic matter, followed by magnesiothermic reduction to produce 3D porous Si. Compared with the reported methods of producing nanostructured Si anodes

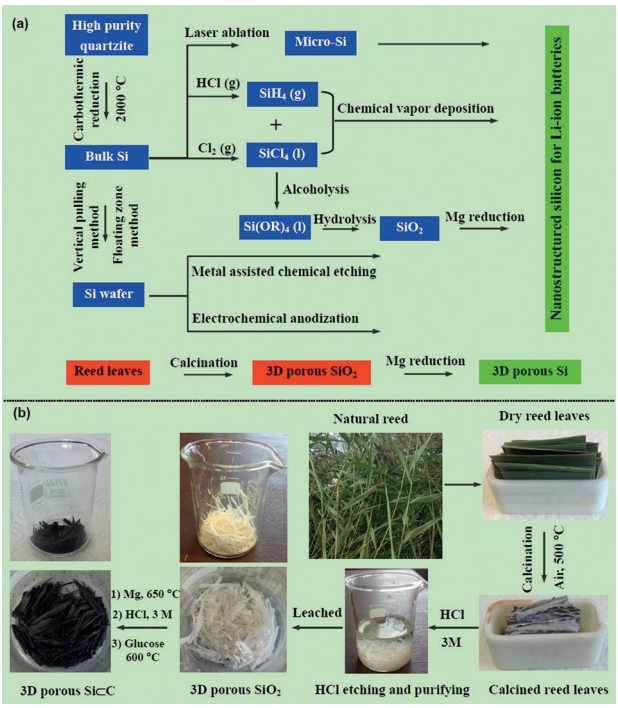

Scheme 1. a) Flow chart showing conventional synthesis routes of nano-Si for Li-ion battery anodes, and along with of our sustainable and low-cost synthesis route from natural reed leaves. b) Detailed flow chart of the process for 3D porous Si⊂C anode from natural reed leaves to the 3D porous SiO_2 precursor and finally the 3D porous Si⊂C anode.

(Scheme 1 a), our developed route has several distinct advantages: 1) reed leaves are sustainable materials source; 2) the recovered silicon retains the favorable 3D silica nanostructure of the reed leaves (which allows for superior battery performance by mitigating pulverization); 3) the overall method is simple; and 4) the overall process does not use expensive Si precursors or reagents. The Mg method used for the reduction process is technologically produced by electrolysis and can be easily regenerated from the $MgCl_2$ by-product.[25] It goes without saying that the use of glucose is sustainable and green as well.

Common reeds from the southwest of Germany (Stuttgart, Baden-Württemberg) are shown in Figure 1 a. They are typical reed plants as found in wetlands of the temperate zones. Figure 1 b,c shows the characteristic leaf texture. Scanning electron microscope (SEM) images at different magnifications as displayed in Figure 1 d,e reveal their hierarchical morphologies. Some microvilli can be observed on the surface of the leaves (Figure 1 e), most of which are surrounded by nanosheets (the inset of Figure 1 e). Optical photos of as-prepared amorphous SiO_2 are shown in Scheme 1 b and in the inset of Figure S1 b (Supporting Information). Compared with original reed leaves (Figure 1 a–c), the retained SiO_2 structure has largely shrunk (Scheme 1 b). The morphology of the as-prepared sample was characterized by SEM (Figure 1 f,g). It retains the original 3D hierarchical structure on the sub-millimeter scale (Figure 1 f; Supporting Information, Figure S1 b), with well-defined uniform patterns. High-magnification SEM image (Figure 1 g) demonstrate that

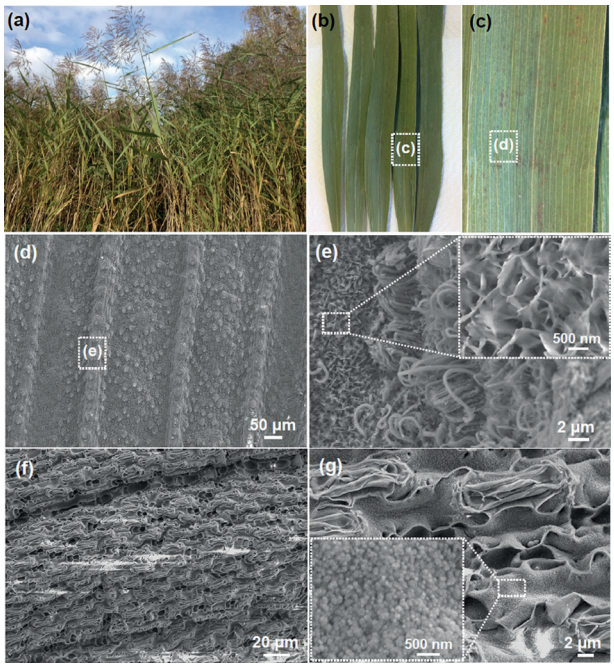

Figure 1. a) Common reeds growing around a river (photo was taken at the Max-Planck Institute for Solid-State Research, Büsnau, Stuttgart, Germany). b) Photograph of the dry reed leaves and c) magnification of the red mark in (b); d,e) SEM images at different magnification of dry reed leaves showing hierarchical and porous structures (the inset); f) low-magnification SEM images showing that the bright white SiO_2 precursor converted from nature reed leaves preserves the original 3D hierarchical microstructure of the reed leaves with large shrinkage; g) high-magnification SEM image clearly display their high porous (inset) and 3D hierarchical microstructures.

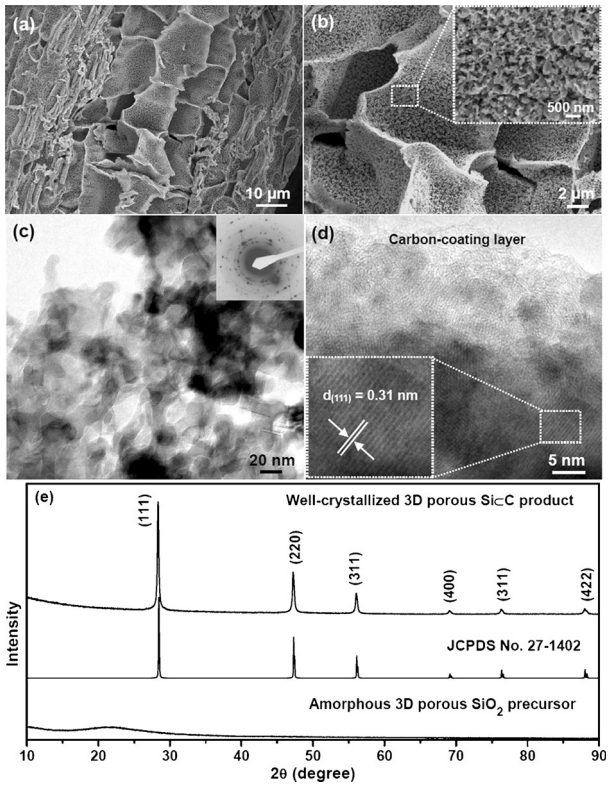

Figure 2. SEM, TEM, and XRD characterizations of the finally achieved highly porous 3D Si⊂C nanostructured anode for Li-ion batteries. a) Low-magnification SEM image revealing that the finally obtained black Si⊂C also inherites the original skeleton morphology of reed leaves and SiO_2 precursor. b) High-magnification SEM image of 3D Si⊂C architecture, showing the highly porous microstructure (inset) after removing the MgO generated in situ during the magnesiothermic reduction process of 3D SiO_2 precursor. c,d) Low-magnification TEM and HRTEM images of 3D Si⊂C displaying the highly porous nanonet architecture, thin carbon-coating, and characteristic lattice spacing of Si (111). e) XRD patterns of the 3D amorphous SiO_2 precursor and well-crystallized 3D highly porous Si⊂C nanonets obtained from the dry reed leaves.

such uniform patterns are wrinkled. The calcined and purified SiO_2 3D architecture is highly porous (the inset of Figure 1 g), which is ascribed to the gas release from the decomposition of organic matters during calcination of reed leaves and impurity leaching in HCl solution. Nitrogen adsorption (Brunauer–Emmett–Teller, BET) measurements (Supporting Information, Figure S2 a,b) indicate that the 3D mesoporous SiO_2 precursor has a BET surface area of 101 $m^2 g^{-1}$ and a total pore volume of 0.22 $cm^3 g^{-1}$.

Figure 2 displays SEM, transmission electron microscopy (TEM), and X-ray diffractometry (XRD) characterizations of the finally achieved 3D highly porous Si⊂C hierarchical architectures. Low-magnification SEM images (Figure 2 a and Figure S1 c in Supporting Information) reveal that even the finally obtained black carbon-coated silicon retains the original skeleton morphology of the reed leaves. The 3D architecture consists of highly porous 2D nanosheets/nanonets (Figure 2 b). As further supported by TEM (Figure 2 c), porous 2D nanosheets/nanonets assemble to the final 3D architecture. High-resolution TEM (HRTEM, Figure 2 d) clearly shows uniform carbon coating, and the characteristic lattice spacing of Si (111) indicates good crystallinity. The uniform carbon coating necessary to improve the otherwise poor electronic conductivity was generated by carbonization of glucose, which was adsorbed on the surface of porous silicon (see the Experimental Section in the Supporting Information). The weight ratio of Si to C was controlled to be 4: 1 via tuning the glucose concentration (see the Supporting Information for details). The complete transformation of porous 3D SiO_2 after magnesiothermic reduction and HCl treatment was also strongly confirmed by XRD measurements (Figure 2 e; Supporting Information, Figure S4). BET surface area measurements were performed for the porous 3D SiO_2 after magnesiothermic reduction and carbon coating, yielding an increased specific surface area of 224 $m^2 g^{-1}$, while the total pore volume was increased from 0.22 $cm^3 g^{-1}$ to 0.70 $cm^3 g^{-1}$ (Supporting Information, Figure S2 c). The pore size distribution curve (Supporting Information, Figure S2 d) demonstrates two types of pores (mesopore and macropore) in the final Si-based products.

Typical cyclic voltammetry (CV) curves of the highly porous Si⊂C anode at a scanning rate of 0.1 $mV s^{-1}$ are shown in Figure 3 a. The weak peak at 0.7 V during the first discharge scan agrees well with the Li-insertion process of crystalline Si to form an amorphous Li_xSi phase.[13] This peak disappears from the second cycle onwards indicating complete amorphization of Si at the end of the first cycle.[13] During the first

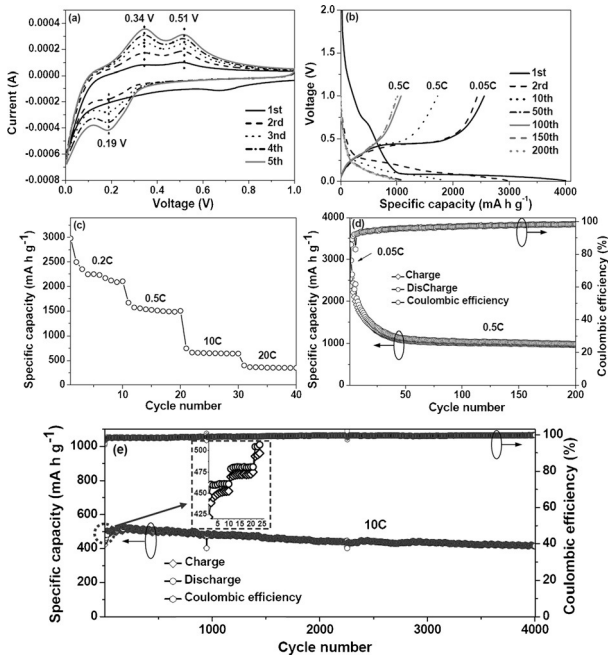

Figure 3. Electrochemical performances of highly porous 3D Si⊂C nanonet anodes. a) CV curves at a scanning rate of 0.1 $mV s^{-1}$ in the voltage range of 0.01–1.0 V. b) voltage–capacity curves at 0.05 C and 0.5 C rates. c) Rate capability at different rates (increased from 0.2 C to 20 C after the first three CV cycles). d) Cycling performances at 0.5 C rate (firstly activated with two cycles at 0.05 C). e) Long-term cycling performance of the highly porous 3D Si⊂C nanonet electrode at a current density of 10 C.

charge process, two distinct peaks are revealed at 0.34 V and 0.51 V, which can be ascribed to the phase transition from Li_xSi to amorphous silicon.[2,26,28] An activation process occurred over the first few cycles, indicated by the increase of the CV peak intensity (Figure 3 a), which is consistent with previous research.[26,28] The galvanostatic discharge–charge process for the 3D porous Si⊂C hierarchical anode was performed in the range of 0.01–1.0 V at a current density of 0.5 C (2 h per half cycle) as shown in Figure 3 b. The first discharge and charge steps deliver a specific capacity of 4000 and 2435 $mA h g^{-1}$, respectively. Note that all the capacity values in the graph were calculated based on Si present in the Si⊂C composites (the values referring to Si⊂C composites and bare Si at various current densities are listed in the Supporting Information, Table S1). As shown in Figure 3 d, though the specific capacity decayed rapidly in the first 50 cycles, the 3D porous Si⊂C anode showed a very stable cycling performance after the first 50 cycles with a specific capacity of about 1100 $mA h g^{-1}$. The discharge capacity remained at a very high level of 1050 $mA h g^{-1}$ even after 200 cycles with high average Coulombic efficiency (Figure 3 d). Discharge–charge curves of the 3D porous Si⊂C anode at different current densities show that they deliver superior rate capability (Figure 3 c). Remarkably, at current densities as high as 10 C and 20 C, this material can still deliver reversible capacities of 745 and 398 $mA h g^{-1}$, respectively. As shown in this figure, the 3D porous Si⊂C anode converted from natural reed leaves displays a high stationary capacity value even under these demanding conditions.

As far as the long cycling behavior of these Si⊂C anode materials for Li-ion batteries is concerned, charge and discharge tests at high current rate were carried out. We examined their cycling performance at a current density of 10 C for as many as 4000 cycles. As shown in Figure 3 e, an electrode capacity of approximate 420 $mA h g^{-1}$ was still retained after 4000 cycles. It is noteworthy that the capacity of the carbon-coated 3D porous Si anode increased during the first 25 charge–discharge cycles (the inset of Figure 3 e), which is consistent with the CV results of the continuous increase of the CV peak intensity in the first five CV cycles (Figure 3 a). After the first 25 cycles, stable cycling performance even at a high current density of 10 C is observed, with high and stable discharge capacities (Figure 3 e). The origin of this activation step in the initial cycle steps may be attributed to the delayed electrolyte wetting of the 3D porous structure of carbon-coated Si electrode.[15] The structure stability of the coated porous Si anode after 200 cycles was also confirmed by SEM (Supporting Information, Figure S5). The 3D porous skeleton of the Si⊂C leaf-shaped electrode is retained, despite the large volume expansion. This observation confirms that the 3D interconnected porous structure and thin carbon-layer coating can reduce the diffusion-induced stress and buffer the volume change during lithiation and delithiation processes,[41–44] contributing to the superior structure stability and good electric contact between Si and carbon.

In conclusion, we have successfully developed a sustainable and low-cost route to highly porous 3D Si⊂C architecture directly from natural reed leaves, in which this topology preexists on the silicate level. The magnesiothermic reduction has two advantages. First it results in a silicon microstructure retaining the original silicic structure. Second, etching of the MgO inclusions leads to a high internal pore density. These features together with the carbon coating of the silicon leads to the attractive electrochemical performance for Li-ion batteries, such as large reversible capacity, high rate capability, and superior cyclability. The 3D hierarchical architecture and 2D highly porous nanosheet/nanonet units buffer the huge volume change, reduce the diffusion-induced stress, and facilitate the diffusion of Li ions and electrolyte into the electrode. The surface carbon coating enhances not only the overall electronic conductivity of Si but also mechanically stabilizes the whole 3D porous structure. Moreover, given the sustainable and facile nature of the synthesis procedure, the described 3D porous Si⊂C nanocomposite has a great potential as a practical anode material for Li-ion batteries.

Keywords: anode materials · carbon coating · lithium-ion batteries · mesoporous silica · reed leaves

How to cite: *Angew. Chem. Int. Ed.* **2015**, *54*, 9632–9636
Angew. Chem. **2015**, *127*, 9768–9772

[1] D. Larcher, J. M. Tarascon, *Nat. Chem.* **2015**, *7*, 19.
[2] B. Dunn, H. Kamath, J.-M. Tarascon, *Science* **2011**, *334*, 928.
[3] J. Maier, *Angew. Chem. Int. Ed.* **2013**, *52*, 4998; *Angew. Chem.* **2013**, *125*, 5100.
[4] N. S. Choi, Z. Chen, S. A. Freunberger, X. Ji, Y. K. Sun, K. Amine, G. Yushin, L. F. Nazar, J. Cho, P. G. Bruce, *Angew. Chem. Int. Ed.* **2012**, *51*, 9994; *Angew. Chem.* **2012**, *124*, 10134.

[5] X. H. Liu, J. W. Wang, S. Huang, F. Fan, X. Huang, Y. Liu, S. Krylyuk, J. Yoo, S. A. Dayeh, A. V. Davydov, S. X. Mao, S. T. Picraux, S. Zhang, J. Li, T. Zhu, J. Y. Huang, *Nat. Nanotechnol.* **2012**, *7*, 749.
[6] K. Ogata, E. Salager, C. J. Kerr, A. E. Fraser, C. Ducati, A. J. Morris, S. Hofmann, C. P. Grey, *Nat. Commun.* **2014**, *5*, 3217.
[7] I. Kovalenko, B. Zdyrko, A. Magasinski, B. Hertzberg, Z. Milicev, R. Burtovyy, I. Luzinnov, G. Yushin, *Science* **2011**, *334*, 75.
[8] F. Du, B. Li, W. Fu, Y. Xiong, K. Wang, J. Chen, *Adv. Mater.* **2014**, *26*, 6145.
[9] H. Wu, G. Chan, J. W. Choi, I. Ryu, Y. Yao, M. T. McDowell, S. W. Lee, A. Jackson, Y. Yang, L. Hu, Y. Cui, *Nat. Nanotechnol.* **2012**, *7*, 310.
[10] C. K. Chan, H. Peng, G. Liu, K. MclWrath, X. F. Zhang, R. A. Huggins, Y. Cui, *Nat. Nanotechnol.* **2008**, *3*, 31.
[11] N. Liu, Z. Lu, J. Zhao, M. T. McDowell, H. Lee, W. Zhao, Y. Cui, *Nat. Nanotechnol.* **2014**, *9*, 187.
[12] X. Li, M. Gu, S. Hu, R. Kennard, P. Yan, X. Chen, C. Wang, M. J. Saior, J. Zhang, J. Liu, *Nat. Commun.* **2014**, *5*, 4105.
[13] H. Kim, B. Han, J. Choo, J. Cho, *Angew. Chem. Int. Ed.* **2008**, *47*, 10151; *Angew. Chem.* **2008**, *120*, 10305.
[14] Y. S. Hu, R. Demir-Cakan, M. M. Titirici, J. O. Muller, R. Schlogl, M. Antonietti, J. Maier, *Angew. Chem. Int. Ed.* **2008**, *47*, 1645; *Angew. Chem.* **2008**, *120*, 1669.
[15] Y. Yu, L. Gu, C. Zhu, S. Tsukimoto, P. A. van Aken, J. Maier, *Adv. Mater.* **2010**, *22*, 2247.
[16] R. Zhang, Y. Du, D. Li, D. Shen, J. Yang, Z. Guo, H. K. Liu, A. A. Elzatahry, D. Y. Zhao, *Adv. Mater.* **2014**, *26*, 6749.
[17] H. Wu, G. Yu, L. Pan, N. Liu, M. T. McDowell, Z. Bao, Y. Cui, *Nat. Commun.* **2013**, *4*, 1943.
[18] A. Magasinski, P. Dixon, B. Hertzberg, A. Kvit, J. Ayala, G. Yushin, *Nat. Mater.* **2010**, *9*, 353.
[19] J. Ji, H. Ji, L. L. Zhang, X. Zhao, X. Bai, X. Fan, F. Zhang, R. S. Ruoff, *Adv. Mater.* **2013**, *25*, 4673.
[20] J. Chang, X. Huang, G. Zhou, S. Cui, P. B. Hallac, J. Jiang, P. T. Hurley, J. Chen, *Adv. Mater.* **2014**, *26*, 758.
[21] C. Wang, H. Wu, Z. Chen, M. T. Mcdowell, Y. Cui, Z. Bao, *Nat. Chem.* **2013**, *5*, 1042.
[22] S. Kondo, K. Tokuhashi, H. Nagai, M. Iwasaka, M. Kaise, *Combust. Flame* **1995**, *101*, 170.
[23] A. Vlad, A. L. M. Reddy, A. Ajayan, N. Singh, J. F. Gohy, S. Melinte, P. M. Ajayan, *Proc. Natl. Acad. Sci. USA* **2012**, *109*, 15168.
[24] Z. Huang, X. Zhang, M. Reiche, L. Liu, W. Lee, T. Shimizu, Z. Senz, U. Gosele, *Nano Lett.* **2008**, *8*, 3046.
[25] X. Sun, H. Huang, K. L. Chu, Y. Zhuang, *J. Electron. Mater.* **2012**, *41*, 2369.
[26] N. Lin, Y. Han, L. Wang, J. Zhou, J. Zhou, Y. Zhu, Y. Qian, *Angew. Chem. Int. Ed.* **2015**, *54*, 3822; *Angew. Chem.* **2015**, *127*, 3893.
[27] N. Liu, K. Huo, M. T. McDowell, J. Zhao, Y. Cui, *Sci. Rep.* **2013**, *3*, 1919.
[28] D. P. Wong, R. Suriyaprabha, R. Yuvakumar, V. Rajendran, Y. T. Chen, B. J. Hwang, L. C. Chen, K. H. Chen, *J. Mater. Chem. A* **2014**, *2*, 13437.
[29] D. S. Jung, M. H. Ryou, Y. J. Sung, S. B. Park, J. W. Choi, *Proc. Natl. Acad. Sci. USA* **2013**, *110*, 12229.
[30] L. Sun, K. Gong, *Ind. Eng. Chem. Res.* **2001**, *40*, 5861.
[31] Z. Favors, W. Wang, H. H. Bay, Z. Mutlu, K. Ahmed, C. Liu, M. Ozkan, C. S. Ozkan, *Sci. Rep.* **2014**, *4*, 5623.
[32] W. S. Kim, Y. Hwa, J. H. Shin, M. Yang, H. J. Sohn, S. H. Hong, *Nanoscale* **2014**, *6*, 4297.
[33] M. J. Hodson, P. J. White, A. Mead, M. R. Broadley, *Ann. Bot.* **2005**, *96*, 1027.
[34] H. A. Currie, C. C. Perry, *Ann. Bot.* **2007**, *100*, 1383.
[35] E. Epstein, *Ann. Appl. Biol.* **2009**, *155*, 155.
[36] J. Zhao, Y. Zhang, T. Wang, P. Li, C. Wei, H. Pang, *Adv. Mater. Interfaces* **2015**, *2*, 1400377.
[37] A. M. Morales, C. M. Lieber, *Science* **1998**, *279*, 208.
[38] D. B. Geohegan, A. A. Puretzky, G. Duscher, S. J. Penyycook, *Appl. Phys. Lett.* **1998**, *72*, 2987.
[39] Y. Cui, L. J. Lauhon, M. S. Gudiksen, J. Wang, C. M. Lieber, *Appl. Phys. Lett.* **2001**, *78*, 2214.
[40] M. Law, J. Goldberger, P. Yang, *Annu. Rev. Mater. Res.* **2004**, *34*, 83.
[41] J. Liu, K. Song, C. Zhu, C. Chen, P. A. van Aken, J. Maier, Y. Yu, *ACS Nano* **2014**, *8*, 7051.
[42] J. Liu, Y. Wen, Y. Wang, P. A. van Aken, J. Maier, Y. Yu, *Adv. Mater.* **2014**, *26*, 6025.
[43] J. Liu, Y. Wen, P. A. van Aken, J. Maier, Y. Yu, *Nano Lett.* **2014**, *14*, 6387.
[44] J. Liu, S. Song, P. A. van Aken, J. Maier, Y. Yu, *Nano Lett.* **2014**, *14*, 2597.

Received: April 7, 2015
Revised: May 5, 2015
Published online: June 26, 2015

